The new vertical Neutron Beam Line at the CERN n_TOF Facility Design and Outlook on the Performance

C. Weiß[a,*], E. Chiaveri[a], S. Girod[a], V. Vlachoudis[a], O. Aberle[a], S. Barros[b], I. Bergström[a], E. Berthoumieux[c], M. Calviani[a], C. Guerrero[d,a], M. Sabaté-Gilarte[d,a], A. Tsinganis[a,e], J. Andrzejewski[f], L. Audouin[g], M. Bacak[h], J. Balibrea-Correa[i], M. Barbagallo[j], V. Bécares[i], C. Beinrucker[k], F. Belloni[c], F. Bečvář[l], J. Billowes[m], D. Bosnar[n], M. Brugger[a], M. Caamaño[o], F. Calviño[p], D. Cano-Ott[i], F. Cerutti[a], N. Colonna[j], G. Cortés[p], M.A. Cortés-Giraldo[d], L. Cosentino[q], L. Damone[j], K. Deo[r], M. Diakaki[e], C. Domingo-Pardo[s], E. Dupont[c], I. Durán[o], R. Dressler[t], B. Fernández-Domínguez[o], A. Ferrari[a], P. Ferreira[b], P. Finocchiaro[q], R. Frost[m], V. Furman[u], S. Ganesan[r], A. Gheorghe[v], T. Glodariu[v], K. Göbel[k], I.F. Gonçalves[b], E. González-Romero[i], A. Goverdovski[w], E. Griesmayer[h], F. Gunsing[c], H. Harada[x], T. Heftrich[k], S. Heinitz[t], A. Hernández-Prieto[a,p], J. Heyse[y], D.G. Jenkins[z], E. Jericha[h], Y. Kadi[a], F. Käppeler[aa], T. Katabuchi[ab], P. Kavrigin[h], V. Ketlerov[w], V. Khryachkov[w], A. Kimura[x], N. Kivel[t], M. Kokkoris[e], M. Krtička[l], E. Leal-Cidoncha[o], C. Lederer[ac,k], H. Leeb[h], J. Lerendegui[d], M. Licata[ad,ae], S. Lo Meo[ae,af], D. López[i], R. Losito[a], D. Macina[a], J. Marganiec[f], T. Martínez[i], C. Massimi[ad,ae], P.F. Mastinu[ag], M. Mastromarco[j], F. Matteucci[ah], E. Mendoza[i], A. Mengoni[af], P.M. Milazzo[ah], F. Mingrone[ad,ae], M. Mirea[v], S. Montesano[a], A. Musumarra[q,ai], R. Nolte[aj], R. Palomo Pinto[d], C. Paradela[o], N. Patronis[ak], A. Pavlik[al], J. Perkowski[f], I. Porras[a,am], J. Praena[d], J.M. Quesada[d], T. Rauscher[an], R. Reifarth[k], A. Riego-Perez[p], M.S. Robles[o], C. Rubbia[a,ak], J. Ryan[m], A. Saxena[r], P. Schillebeeckx[y], S. Schmidt[k], D. Schumann[t], P. Sedyshev[u], G. Smith[m], A. Stamatopoulos[e], P. Steinegger[t], S.V. Suryanarayana[r], G. Tagliente[j], J.L. Tain[s], A. Tarifeño-Saldivia[s], L. Tassan-Got[g], S. Valenta[l], G. Vannini[ad,ae], V. Variale[j], P. Vaz[b], A. Ventura[ae], R. Vlastou[e], A. Wallner[ao], S. Warren[m], M. Weigand[k], T. Wright[m], P. Žugec[n],
(The n_TOF Collaboration (www.cern.ch/ntof))

[a] *European Organization for Nuclear Research (CERN), Geneva, Switzerland*
[b] *Instituto Tecnológico e Nuclear, Instituto Superior Técnico, Universidade Técnica de Lisboa, Lisboa, Portugal*
[c] *Commissariat à l'Énergie Atomique (CEA) Saclay - Irfu, Gif-sur-Yvette, France*
[d] *Universidad de Sevilla, Spain*
[e] *National Technical University of Athens (NTUA), Greece*
[f] *Uniwersytet Łódzki, Lodz, Poland*
[g] *Centre National de la Recherche Scientifique/IN2P3 - IPN, Orsay, France*
[h] *Atominstitut, Technische Universität Wien, Austria*
[i] *Centro de Investigaciones Energeticas Medioambientales y Tecnológicas (CIEMAT), Madrid, Spain*
[j] *Istituto Nazionale di Fisica Nucleare, Bari, Italy*
[k] *Johann-Wolfgang-Goethe Universität, Frankfurt, Germany*
[l] *Charles University, Prague, Czech Republic*
[m] *University of Manchester, Oxford Road, Manchester, UK*
[n] *Department of Physics, Faculty of Science, University of Zagreb, Croatia*
[o] *Universidade de Santiago de Compostela, Spain*
[p] *Universitat Politecnica de Catalunya, Barcelona, Spain*
[q] *Istituto Nazionale di Fisica Nucleare, Laboratori Nazionali del Sud, Catania, Italy*
[r] *Bhabha Atomic Research Centre (BARC), Mumbai, India*
[s] *Instituto de Física Corpuscular, CSIC-Universidad de Valencia, Spain*
[t] *Paul Scherrer Institut, Villigen PSI, Switzerland*
[u] *Joint Institute for Nuclear Research (JINR), Dubna, Russia*
[v] *Horia Hulubei National Institute of Physics and Nuclear Engineering - IFIN HH, Bucharest - Magurele, Romania*
[w] *Institute of Physics and Power Engineering (IPPE), Obninsk, Russia*
[x] *Japan Atomic Energy Agency (JAEA), Tokyo, Japan*
[y] *European Commission JRC, Institute for Reference Materials and Measurements, Retieseweg 111, B-2440 Geel, Belgium*
[z] *University of York, Heslington, York, UK*
[aa] *Karlsruhe Institute of Technology, Campus Nord, Institut für Kernphysik, Karlsruhe, Germany*
[ab] *Tokyo Institute of Technology, Tokyo, Japan*
[ac] *School of Physics and Astronomy, University of Edinburgh, Edinburgh, UK*
[ad] *Dipartimento di Fisica e Astronomia, Università di Bologna, Italy*
[ae] *Istituto Nazionale di Fisica Nucleare, Bologna, Italy*
[af] *Agenzia nazionale per le nuove tecnologie, l'energia e lo sviluppo economico sostenibile (ENEA), Bologna, Italy*
[ag] *Istituto Nazionale di Fisica Nucleare, Laboratori Nazionali di Legnaro, Italy*
[ah] *Istituto Nazionale di Fisica Nucleare, Trieste, Italy*
[ai] *Dipartimento di Fisica e Astronomia, Università di Catania, Italy*
[aj] *Physikalisch Technische Bundesanstalt (PTB), Braunschweig, Germany*
[ak] *University of Ioannina, Ioannina, Greece*
[al] *University of Vienna, Faculty of Physics, Austria*

[*] Corresponding author
Email address: christina.weiss@cern.ch (C. Weiß)

[am] University of Granada, Spain
[an] University of Hertfordshire, Hertfordshire, UK
[ao] Australian National University, Canberra, Australia

Abstract

At the neutron time-of-flight facility n_TOF at CERN a new vertical beam line was constructed in 2014, in order to extend the experimental possibilities at this facility to an even wider range of challenging cross-section measurements of interest in astrophysics, nuclear technology and medical physics. The design of the beam line and the experimental hall were based on FLUKA Monte Carlo simulations, aiming at maximizing the neutron flux, reducing the beam halo and minimizing the background from neutrons interacting with the collimator or back-scattered in the beam dump.
The present paper gives an overview on the design of the beam line and the relevant elements and provides an outlook on the expected performance regarding the neutron beam intensity, shape and energy resolution, as well as the neutron and photon backgrounds.

Keywords: n_TOF facility, Neutron time-of-flight, FLUKA, neutron cross-section measurement

1. Introduction

The neutron time-of-flight facility n_TOF at CERN [1, 2] is a pulsed white neutron source for high-accuracy neutron cross-section measurements over a wide neutron energy range. The neutrons are produced in a monolithic Pb-spallation target, where a pulsed 20 GeV/c proton beam provided by the CERN Proton Synchrotron (PS) [3] impinges with a maximum repetition rate of 0.8 Hz. The primary proton beam has a width of rms = 7 ns. The Pb-target is surrounded by an additional moderator layer, to generate a neutron beam with energies ranging from thermal up to several GeV. At the facility in operation since 2000 the measurements take place in an experimental area placed at the end of a horizontal beam line, 200 m in length. The experimental conditions and neutron beam characteristics at this horizontal flight path are presented in full detail in reference [4].
The horizontal 200 m flight path, with its record instantaneous neutron beam intensity, has allowed very important cross-sections to be measured, getting unprecedented energy resolution in both neutron capture [5, 6] and fission [7] as well as extending the measurement range to previously unreachable neutron energies [8]. However, there are more challenging experiments that require an even more intense neutron beam.
In order to extend the experimental possibilities at the n_TOF facility for cross-section measurements of very low mass samples (< 1 mg), reactions with small cross-sections or highly radioactive samples [9], an additional vertical flight path of 20 m with a significantly higher neutron flux was designed and constructed in 2014. The design and implementation of this new beam line, with an outlook on the expected performance are the subject of this paper. In Section 2 the final beam line configuration, as in operation at CERN since July 2014, is presented with a description of the different elements. The expected characteristics of the neutron beam and the background conditions, determined by means of FLUKA Monte Carlo simulations, are discussed in Section 3.

2. General Layout and technical Description

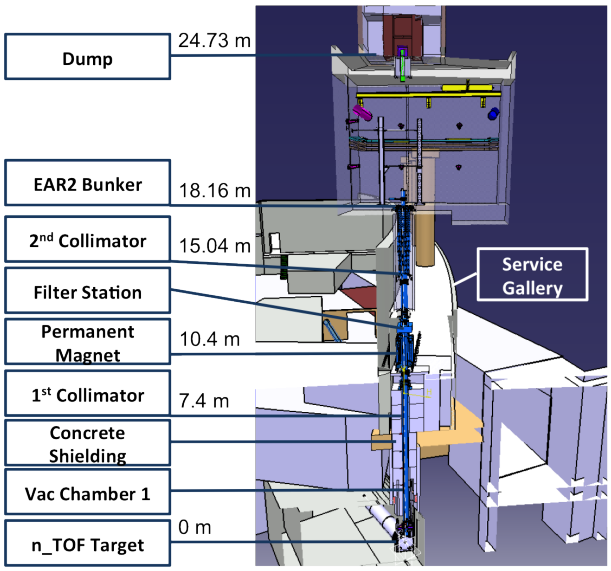

Figure 1: General layout of the vertical flight path, from the spallation target to the beam dump. The different beam line elements with the position of their entrance are indicated on the left.

The n_TOF spallation target is installed in the TT2A tunnel at CERN. The spallation target was lowered to its current position through an existing vertical shaft via a service gallery. This shaft was now used to install the bottom part of the vertical beam line which is presented here. From the roof of the service gallery, at 12.6 m from the target center, to the ground, a new concrete shaft with an inner diameter of 800 mm was built during 2013. At ground level, 18.16 m above the spallation target, a new building was constructed, hosting the bunker with the experimental area, an electronics room and two preparatory rooms. The beam dump for this new vertical flight path is installed on the roof of the bunker. The existing service gallery is used to house the magnet and the filter box of the beam line, as

well as to allow the access to the 1st collimator.
The general layout with the different beam line elements is shown in Figure 1. The distance to the spallation target center for the different beam line elements, which are described in further detail below, are listed in Table 1.

Table 1: Beam line elements and their position with respect to the center of the n_TOF spallation target.

Beam Line Element	Distance to target center [m]
1st collimator	7.4 - 8.4 (d = 200 mm)
Magnet center	10.4
Filter box	11.4
2nd collimator	15.04 - 18.04 (d = 70 - 21.8 mm)
Experimental area	18.16 - 23.66
Beam dump	24.73

2.1. The Beam Line at the Level of the Spallation Target

The n_TOF spallation target consists of a Pb cylinder 400 mm in length and 600 mm in diameter, surrounded by a layer of demineralized water acting as coolant and, only in the forward direction, an additional moderator layer, usually filled with borated water in saturation. The target is surrounded by an Al container and supported by an Al alloy structure. The support structure has a polygonal opening on the top, to allow the lowering of a vacuum chamber for the vertical beam line down to the level of the target.
The vacuum line of the vertical beam line has therefore a polygonal section for the first 0.9 m, after which it opens to a circular beam pipe with 317 mm inner diameter. The neutron window at the bottom of the polygonal section is concave, to match the shape of the spallation target. The neutron window at this level is 1.5 mm in thickness and made of Al, leaving a gap of 10 mm air between the window and the Al-housing of the target. Due to technical constraints, the window is installed off-center with respect to the center of the spallation target, as shown in Figure 2. The reference point, marking the center of the circular beam pipe above, is 49 mm downstream and 100 mm to the right with respect to the target center and the direction of the impinging proton beam.

2.2. Collimation System

The neutron beam is shaped by two collimators:

- The 1st collimator is installed at 7.4 m above the target inside the first vacuum pipe of the beam line. It consists of a 1 m long Fe cylinder with 200 mm inner diameter. It is suspended from the service gallery on 1.1 m long rods, attached to a ring at the top of the corresponding vacuum chamber.

- The 2nd collimator is installed at 15.04 m above the target, inside a large vacuum vessel with 680 mm outer diameter. The vacuum vessel is suspended just below the floor of the experimental hall. The different sections of the collimator are resting on 4 steps inside this vacuum vessel. These steps serve as chicanes, avoiding the streaming of neutrons to the experimental hall outside the beam.
The collimator consists of 2 m Fe and 1 m borated polyethylene (B-PE), where the last 0.4 m have a core of boron-carbide (B_4C) cylinders. The inner dimensions of the collimator follow a step geometry, to approximate a conical design. The inner diameters of the different steps are listed in Table 2. The last section of this collimator is shown in Figure 3, where the inner and outer step design are noticeable.

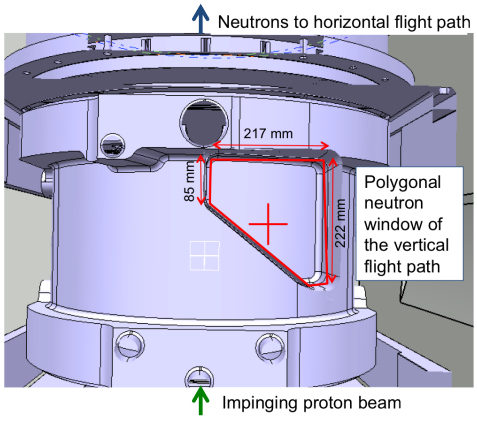

Figure 2: Model of the n_TOF spallation target seen from the top. The proton beam is impinging from the lower edge on the picture. The neutron beam towards the horizontal beam line leaves the target in the forwards direction. The neutron window and the polygonal section of the vertical beam line are indicated on the right. The reference point in red (cross) marks the center of the vertical beam line.

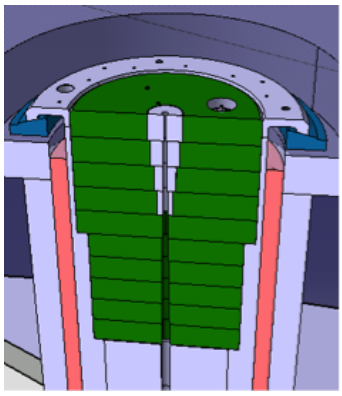

Figure 3: Last meter of the second collimator installed inside the big vacuum vessel which is supported 120 mm below the EAR2 floor. The B-PE part is shown in green with the B_4C core in the last 400 mm in light blue. The stainless steel spheres, installed around the vacuum vessel for shielding purposes, are indicated in light red. The first two steps inside the vacuum vessel, on which the collimator rests, are visible at the sides of the collimator.

The exit of the second collimator is situated 120 mm below the floor of the experimental area. Due to the geometry of the collimation system and the close distance to the target, the neu-

Table 2: Inner diameters (d) and material of the different sections of the 2^{nd} collimator. The position is given in distance to the spallation target center.

Position [m] (± 0.002)	Material	d [mm] (± 0.2)
15.04 - 15.29	Steel	70.0
15.29 - 15.54	Steel	66.0
15.54 - 15.79	Steel	61.8
15.79 - 16.04	Steel	57.6
16.04 - 16.29	Steel	53.4
16.29 - 16.54	Steel	49.4
16.54 - 16.79	Steel	45.2
16.79 - 17.04	Steel	41.0
17.04 - 17.14	B-PE	36.8
17.14 - 17.24	B-PE	35.2
17.24 - 17.34	B-PE	33.4
17.34 - 17.44	B-PE	31.8
17.44 - 17.54	B-PE	30.2
17.54 - 17.64	B-PE	28.4
17.64 - 17.74	B_4C	26.8
17.74 - 17.84	B_4C	25.2
17.84 - 17.94	B_4C	23.4
17.94 - 18.04	B_4C	21.8

tron beam halo is diverging by 1 mm over 100 mm distance to the 2^{nd} collimator exit, inside the experimental area. The focal point, which is theoretically the position of the narrowest spatial beam profile, is positioned at 1.08 m from the floor of the experimental area (EAR2).

2.3. Shielding

Various shielding elements are installed along the beam line. In their design, special care was taken to allow the dismantling of the beam line, in order to leave the spallation target accessible for future upgrades and consolidation activities. The gaps between the vacuum pipes and the shielding elements are minimized as much as mechanically possible.
The beam line shielding up to the experimental area consists of the following elements:

- Shielding around the bottom part of the beam line: From 0.9 m above the spallation target, up to the floor of the service gallery at 9.8 m, concrete shielding elements are placed. Up to 7 m above the target the ducts for the cooling system of the spallation target are installed in the same shaft as the beam line. The concrete shielding elements at this level have recesses to let these ducts pass.
  Above the position of the first collimator, at about 9 m from the target, an additional Fe collar was installed around the beam pipe in addition to the concrete shielding, to enhance the shielding at this level and reduce the radiation level on the permanent magnet, which is installed just above in the service gallery.

- Shielding around the middle part of the beam line: From the roof of the service gallery at 12.6 m to the exit of the second collimator at 18.4 m, the beam line shielding mainly consist of 4 tons of stainless steel spheres, 4.8 mm in diameter, filling the volume between the vacuum vessel containing the second collimator and the shaft walls. The spheres can be removed by a special retaining system at the roof of the service gallery.
  An additional concrete ring 1.5 m in length and with an inner diameter of 480 mm is installed in the shaft below the big vacuum vessel.

- At the floor of the experimental area, 0.1 m thick plates of Lithium-Polyethylene (Li-PE) are installed around the beam pipe, covering the area of the shaft below, to absorb thermalized neutrons.

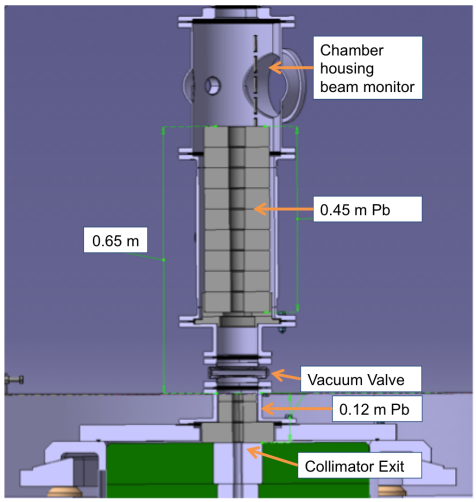

Figure 4: Pb shielding after the second collimator as installed by default inside the first vacuum chambers in the experimental area. The section which contains the vacuum valve is left without additional shielding.

In addition to the beam line shielding, additional elements are installed inside the experimental area to reduce the background contributions to the measurements.

- Right after the exit of the second collimator, Pb disks are installed inside the vacuum chambers to reduce γ-background coming from the last section of the collimator. The inner diameters of the Pb disks are matched to the diverging beam and can hence be understood as an extension of the collimation system. The length of this Pb-shielding can be adjusted to the needs. In Figure 4 the default configuration of this shielding 0.57 m in effective height are indicated.

- In the last vacuum pipe of the beam line, which is fixed to the roof of the bunker just before the beam dump, a removable shielding of 1 m length is installed, indicated in Figure 5 in green. These shielding elements are designed to reduce photons and neutrons streaming back from the beam dump to the experimental setup. Their dimensions match the beam optics at the entrance of the beam dump, within 5 mm.

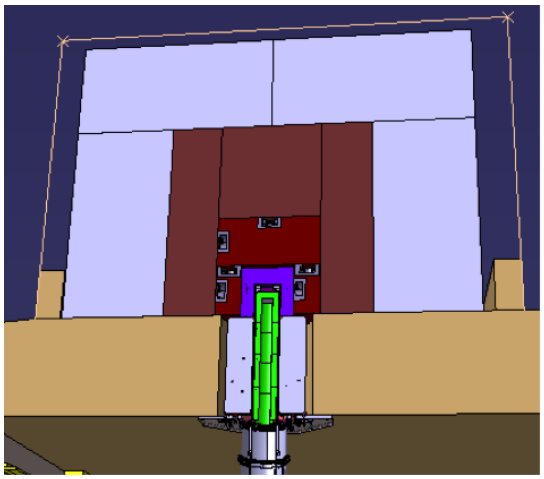

Figure 5: Beam dump and last part of the EAR2 beam line. The last vacuum chamber contains additional shielding material (green) to reduce the background to the experiment from backscattered neutrons and photons. This chamber is installed in the roof of the building and penetrates the core of the beam dump. The beam dump, which is installed on the roof of the building contains three layers, as explained in the text.

- A 50 mm Pb disk is positioned just below the last window before the beam dump.
- B-PE cylinders with an inner diameter of 200 mm are inserted in the vacuum chamber below the Pb disk, over a length of 0.95 m.
- B_4C cylinders with an inner diameter of 150 mm are inserted additionally into the B-PE cylinders.

2.4. Beam Dump

The beam dump is installed on the roof of the building. It consists of three layers to fully absorb the neutron beam and to respect the dose rate for low-occupancy areas, 2.5 μSv/h, outside the building. The beam dump was designed to respect these limits for radiation protection even for a large diameter beam produced with a 2^{nd} collimator having an exit diameter of 200 mm instead of the current 21.8 mm.

- The core of the beam dump consists of a block of B-PE to slow down and to capture neutrons, both from the primary impinging beam and neutrons which are backscattered from the consecutive beam dump layers. The outer dimensions of the core are 400 x 400 x 400 mm^3. The B-PE block has a cylindrical hole at the entrance, 250 mm in height and 340 mm in diameter, where the last vacuum chamber of the beam line is inserted.
- The B-PE core is surrounded by Fe blocks to absorb the fast neutrons and photons of the beam. The outer dimensions of the Fe part is 1600 x 1600 x 1600 mm^3.
- The beam dump is finally shielded by concrete with outer dimensions of 3200 x 3200 x 2400 mm^3.

Figure 5 shows a cut through the 3D model of the last part of the EAR2 beam line. The removable shielding elements inserted in the last vacuum pipe, which extends inside the first part of the beam dump, are indicated in green.

2.5. Permanent Magnet

To deflect all charged particles which originate from the spallation process in the Pb-target before the experimental hall, a permanent dipole magnet is installed 10.4 m above the spallation target [10]. The magnet poles consist of an assembly of 168 Sm_2Co_{17} radiation resistant permanent magnet blocks, with additional iron poles to smooth possible deviations of the magnetization direction of the permanent magnet blocks. The installation of additional Sm_2Co_{17} blocks on each side of the gap compensates radial stray field losses and improves the integrated field homogeneity. The assembly is installed inside a steel return yoke.
The dipole magnet has an inner gap of 340 mm, where the vacuum pipe of the beam line is installed. The magnetic field in the center of the magnet is 0.253(4) T, over the total dipole length of 1.134 m. The integrated field of the magnet is 0.287 Tm.
The design constraints for the dipole magnet were based on the expected charged particle spectra from FLUKA simulations in the experimental hall. The results of these simulations are shown in Figure 6. To deflect all charged particles from the beam, a minimum integrated field of 0.2 Tm was calculated for the nominal magnet position, given the maximum momentum of 1.205 GeV/c for protons.

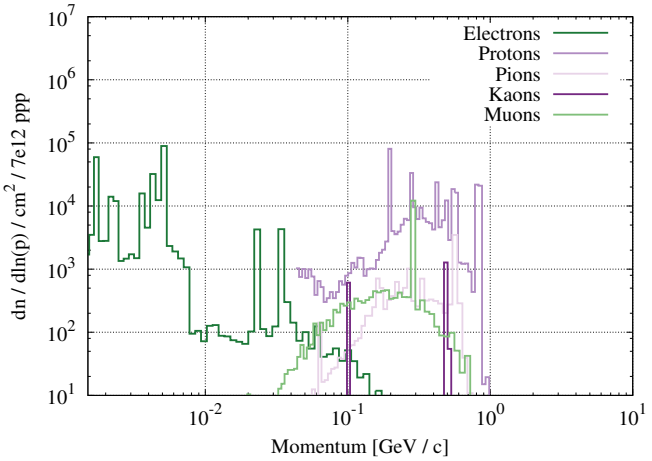

Figure 6: Resulting charged particle spectra in the experimental hall from FLUKA simulations if no magnet is installed in the beam line. The results are normalized to a nominal proton beam intensity at n_TOF of $7 \cdot 10^{12}$ protons per pulse (7e12 ppp). The maximum momentum for protons is 1.205 GeV/c.

2.6. Neutron Filters

A neutron filter station is installed 11.4 m above the spallation target. It contains 8 filters which can be individually inserted into the neutron beam to blank out different neutron energies from the beam or attenuate the in-beam photons. The filter station is remotely controlled from the n_TOF control room.

The available filters and the neutron energy of the corresponding black resonances are listed in Table 3.

Table 3: Neutron filters installed in the filter box. The thickness of the materials is given in brackets after the chemical element. All filters are 215 x 215 mm^2 in area and mechanically supported only on the edges.

Slot #	Filter material (Thickness [mm])	Resonance energy [eV]
1	Mo (10)	45
	W (8.0)	4, 19,184
	Co (0.25)	132
2	Ag (0.50)	5.2
3	Bi (50)	800, 2300
4	Cd (0.50)	thermal cut-off
5	Al (30)	5900, 35100
6	Al (80)	5900, 35100
7	Pb (20)	γ-attenuation
8	Pb (10)	γ-attenuation

2.7. Experimental Area (EAR2)

The bunker housing the experimental area, where the measurements take place, has the floor located at a distance of 18.16 m with respect to the center of the target, while the ceiling is at 23.66 m. The beam line elements from 0.2 - 3 m above the floor of the area are easily exchangeable to meet the requirements of the different experiments. By default, the first meter is reserved for the Pb shielding and a neutron flux monitor, which are installed inside the vacuum pipes in the lowest section of the experimental station. Removable vacuum pipes can be mounted along the beam line, with sizes matching the dimension of the beam in order to allow a close geometry during capture measurements, as illustrated in Figure 7 where the experimental setup during background measurements is shown.

A set of versatile support structures is available for the different detection systems in use, which are mounted on a pillar system in the area. For capture measurements a remotely controlled sample changer is mounted, to allow the change of the samples during beam time.

The bunker is equipped with all necessary systems to be operated as Class A laboratory [11]. A dedicated ventilation system keeps an under-pressure of −150 Pa with respect to atmospheric pressure inside the experimental area, whereas the changing room and the electronics room are held at -50 Pa and -100 Pa respectively, ensuring an appropriate dynamic confinement.

3. Simulations and Expected Performance

The beam line design of the vertical flight path was based on extensive Monte Carlo simulation studies [12, 13], which were performed with the FLUKA code [14, 15], using the graphical interface FLAIR [16]. The simulations focused especially on:

1. Studying the beam characteristics inside the experimental area for different collimation systems.

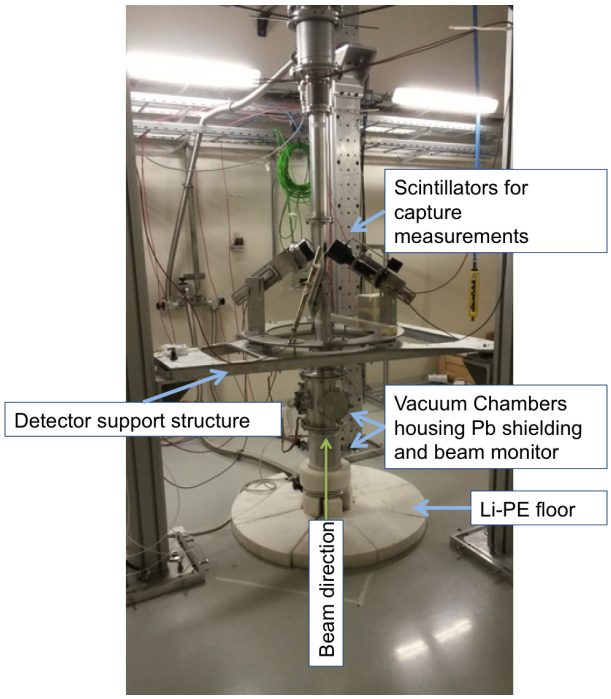

Figure 7: The experimental station during background measurements with scintillators.

2. Investigating experimental conditions for cross-section measurements with various shielding compositions, in particular background simulations for capture experiments with scintillators.
3. Evaluating radiation levels in areas neighboring the beam line and the bunker, which have to comply with the official CERN dose rate limits [17] for accessible zones.

In order to reduce the computing time for the various different configurations, a two step approach was adopted in the simulations. The spallation target with the impinging proton beam was simulated in a first step to retrieve the information about particles exiting the target in the vertical direction. These particles were used as source in the following simulations of different beam line configurations.

The expected beam characteristics and experimental conditions with the above presented beam line are discussed in the following.

3.1. Neutron Flux Spectrum

The neutron flux spectrum, which represents the number of neutrons per impinging proton pulse on the spallation target as a function of neutron energy E_n, was simulated in the nominal sample position 1.6 m from the floor of the experimental area. As discussed in the next section, at this position the neutron beam profile has a full width at half maximum (FWHM) of 21 mm. In order to cover the full spatial beam profile, the simulated neutron flux was integrated over a surface 100 mm in diameter to obtain the total number of neutrons. The results were normalized to the nominal proton beam intensity of 7x10^{12} protons per pulse (ppp) at n_TOF.

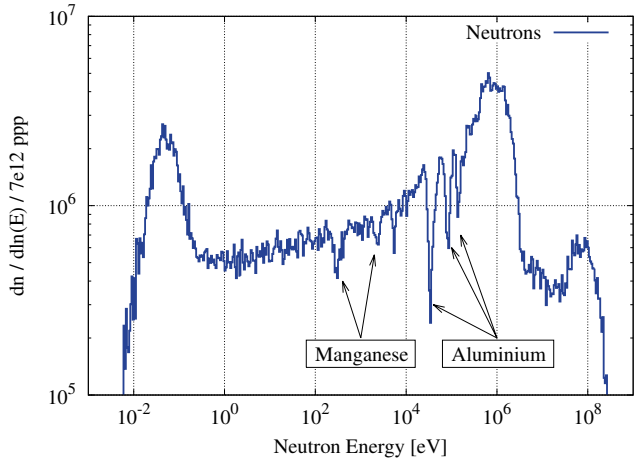

Figure 8: Simulated neutron flux at a nominal sample position in the experimental area. The dips in the spectrum are due to a significant amount of Al with traces of Mn at the spallation target. The spectrum is normalized to the nominal proton beam intensity at n_TOF, $7x10^{12}$ protons per pulse.

Table 4: Integrated neutron flux for different neutron energy decades, normalized to $7x10^{12}$ protons per pulse, for both experimental areas at n_TOF. The evaluated neutron fluence at the horizontal flight path (EAR1) corresponds to the capture measurement setup with pure water as moderator from reference [4]. For neutron energies in the keV range the expected neutron flux is up to a factor 26 higher at the vertical flight path.

Neutron Energy	EAR2 FLUKA Neutrons / Pulse	EAR1 Evaluated Neutrons / Pulse
10 - 100 meV	1.5 x 10^6	1.0 x 10^5
0.1 - 1 eV	6.7 x 10^5	4.3 x 10^4
1 - 10 eV	5.2 x 10^5	2.7 x 10^4
10 - 100 eV	6.2 x 10^5	2.8 x 10^4
0.1 - 1 keV	6.8 x 10^5	2.9 x 10^4
1 - 10 keV	8.6 x 10^5	3.2 x 10^4
10 - 100 keV	1.2 x 10^6	4.4 x 10^4
0.1 - 1 MeV	3.0 x 10^6	1.3 x 10^5
1 - 10 MeV	1.7 x 10^6	1.5 x 10^5
10 - 100 MeV	4.7 x 10^5	5.0 x 10^4
0.1 - 1 GeV	1.6 x 10^5	4.7 x 10^4
Total	1.1 x 10^7	6.8 x 10^5

The total flux energy distribution is illustrated in Figure 8. The neutron evaporation peak is visible in the spectrum around $E_n = 1$ MeV. The strong dips in the spectrum in the region 20 keV $< En <$ 200 keV are due to the significant amount of Al at the target level in the upwards direction. Additional dips are observed at 300 eV and 2 keV due to Mn traces in the aluminum-alloy used for the structural elements at the target. The peak at low neutron energies results from the thermalization of the neutrons in the water surrounding the spallation target.

The integrated flux for different neutron energy decades is listed in Table 4. The total number of neutrons per proton pulse is $1.1x10^7$ neutrons per $7x10^{12}$ protons impinging on target. For comparison, the evaluated neutron fluence at the horizontal flight path at n_TOF (EAR1) [4], for a 2^{nd} collimator exit of d=18 mm for capture measurements and pure water as moderator, is listed as well in Table 4. The highest neutron gain at the vertical flight path is a factor 26 in the energy interval $1 < E_n < 10$ keV.

In Figure 9 the neutron flux is shown as a function of time-of-flight (TOF), together with the in-beam photon background. The corresponding E_n are indicated with arrows for some TOF values. The in-beam photon spectrum is discussed in further detail in Section 3.3, together with the photon energy spectra for the prompt and delayed photons.

3.2. Neutron Beam Profile

The neutron beam profile is dictated by the geometry and distance of the 1^{st} and 2^{nd} collimator in the beam line. The focussing lines define the focal point, which is 1.08 m above the floor of the experimental area. The defocussing lines of the geometry define the size of the beam halo along the height of the experimental area. For the presented configuration, the halo is diverging by 1 mm over 0.1 m increasing distance to the target. The nominal sample position for capture measurements is located at 1.6 m from the floor of the bunker, as the best compromise between beam profile and background conditions was found for this height. At this position the neutron beam width is 21 mm FWHM. In Figure 10 the projected neutron beam profile for thermal neutron energies at different heights in the experimental room is shown, with the profile at the nominal sample position drawn in ochre. The profile of the neutron beam at 6.6 m from the floor of the experimental area corresponds to the beam profile at the entrance to the beam dump.

The neutron beam profile for different TOF decades is illustrated in Figure 11, for the nominal sample position. The beam halo at this position is 50 mm in diameter, which is slightly less than the 55 mm expected from the optical considerations. The neutron background outside the beam is 4 – 5 orders of magnitude lower than at the peak of the beam profile.

Due to the small opening of the 2^{nd} collimator, exact simulations of the beam profile are difficult to retrieve from Monte Carlo simulations for this geometry. Additional simulations of a large 2^{nd} collimator, having a diameter of 50 mm at the exit, have shown that the neutron beam for $E_n > 1$ MeV is asymmetric. A mirrored projection of the polygonal window above the neutron target can be observed in the beam profile at these high neutron energies. This is expected to be visible as well with the currently presented collimator geometry.

3.3. Background Conditions

To estimate the background conditions, the in-beam photon background was studied as well as the contributions coming from different beam line elements and the bunker.

3.3.1. In-beam Photon Background

The in-beam photon background, i.e. the gamma-rays traveling with the neutron beam can be divided in two parts:

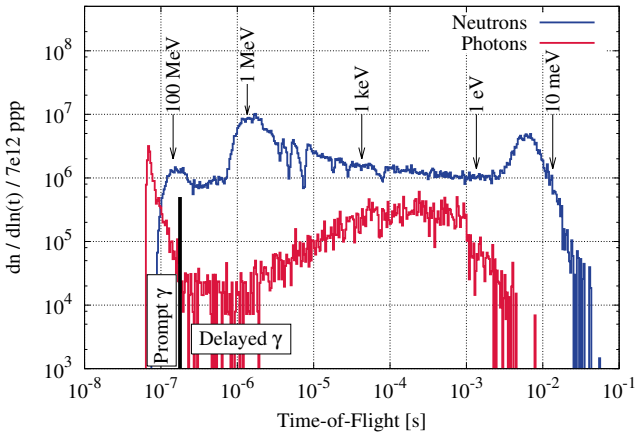

Figure 9: Neutron and photon fluence as function of TOF at the nominal sample position in the experimental area. The corresponding E_n is indicated for different energies with arrows. The in-beam photon spectrum can be divided in prompt and delayed γ.

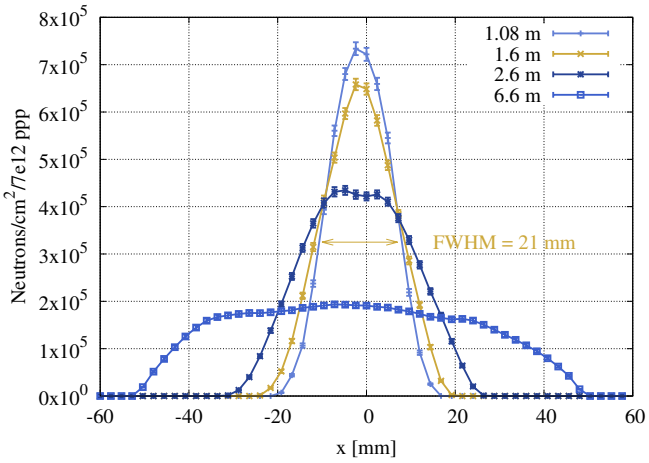

Figure 10: Neutron beam profile projections at different heights in the experimental area, for thermal neutron energies. The heights are given as distance to the floor of the experimental hall. The beam profile at the nominal capture sample position, 1.6 m from the floor, has FWHM = 21 mm. The neutron beam enters the beam dump at 6.6 m from the floor.

- Prompt γ, originating from the spallation process in the target, arrive at the experimental area in the first 200 ns, as indicated in Figure 9. These photons are the main contributors to the so-called 'γ-flash', the first signal detected by most of the detectors in the experimental area. As shown in Figure 12, the photon energies E_γ are ranging up to a few hundred MeV, where the dominant part is below 10 MeV.

- Delayed γ, originating from the moderation process at the target, are arriving at the experimental station up to 5 ms after the γ-flash. The dominant E_γ is 2.2 MeV, from photons generated by neutron capture reactions on the ^{1}H isotopes present in the cooling water of the target. Additional peaks are observed in the E_γ-spectrum at 511 keV, from e^-+e^+ annihilation, and in the range of 7 - 7.5 MeV, from capture reactions in the target and surrounding materials (Pb, Fe and Al).

The detailed E_γ spectra of the in-beam photon background are displayed in Figure 12.

3.3.2. Background Contribution from Beam Line Elements

Extensive studies have been performed to estimate the different background contributions coming from the beam line elements and the experimental hall. A volume containing C_6D_6 liquid, a standard detector type for capture measurements at n_TOF, was included in the FLUKA geometry around the beam pipe at 1.5 m above the floor of the experimental area, corresponding to the nominal position of the detectors, which are usually placed upstream of the capture sample. The energy deposition by different particles in this volume was studied with various shielding configurations to estimate the expected background conditions. A detailed discussion on the simulation results is published in Reference [18]. These background simulations have led to the design of the various shielding elements and the choice for the materials in use in the 2^{nd} collimator.
The results show that, in absence of shielding elements along the beam line in the bunker, about 30% of the background originates from backscattered particles from the beam dump. The remaining part of the background is caused by particle interactions at the exit of the collimator. 35% of the background is caused directly from particles streaming to the detector from the exit of the collimator and the remaining 35% are contributed indirectly from backscattered radiation from the walls of the bunker. The shielding elements discussed in Section 2.3 were introduced in order to reduce the background originating from the beam dump and directly from the 2^{nd} collimator.
The influence of mylar windows and air around the sample position on the energy deposition in the C_6D_6 detectors was studied as well and it was confirmed that the air gap contributes more with increasing distance between the mylar windows at the vacuum-air interface.
The energy deposition in the C_6D_6 volume in the final beam line configuration and with a realistic experimental setup, including two Mylar windows and an air gap of 50 mm at the sample position, for 10 μs < TOF < 100 μs, is expected to be E_{dep} = 53.9 keV/cm^3 ± 5% in total, where 22.5 keV/cm^3 is due to the neutron background.

3.4. Neutron Energy Resolution

At a neutron time-of-flight facility the kinetic energy of the neutron is determined by measuring the time from the primary beam impinging on the target to the detection of the signals coming from neutron-induced reactions at the measuring station and converting the resulting TOF to E_n. Because of the neutron creation and moderation processes at the target and the width of the impinging primary proton beam on the target, the relation between TOF and E_n is represented by distributions of a particular shape, rather than constant values.

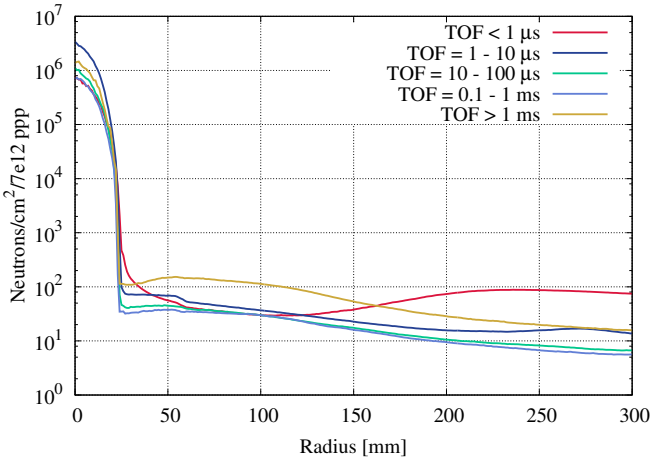

Figure 11: Neutron beam profile projections for different TOF ranges at 1.6 m from the floor of the experimental area. With all shielding elements installed, the neutron background is 4 - 5 orders of magnitude smaller than the peak of the profile.

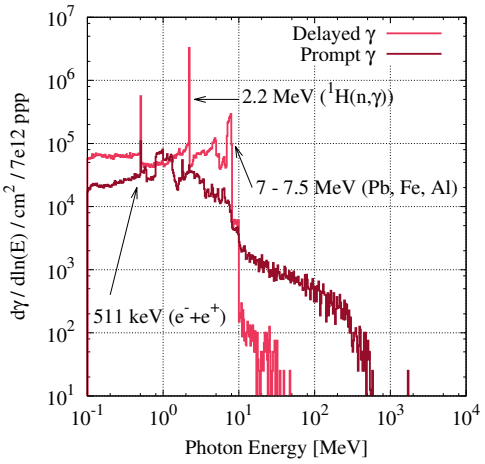

Figure 12: Photon energy spectra of the in-beam γ in the experimental area. The spectrum for prompt γ corresponds to photons arriving in the first 200 ns at the experimental station, the main contribution to the so-called 'γ-flash' in the detectors.

This relation of TOF and E_n for the vertical direction at the n_TOF spallation target is illustrated in Figure 13, where the influence of the proton beam time spread (7 ns rms) is not included. Neutrons of a given energy E_n arrive at the measurement position with a specific time distribution, with the shape of the distribution changing with E_n. These distributions represent the resolution function of the facility. The resolution function has to be well known for the high accuracy determination of cross-sections. It can only be determined by extensive Monte Carlo simulations, which are consecutively validated via experiments.

The time distributions can equivalently be expressed in length, where the effective flight path of the neutron is the sum of the geometrical flight path L and an equivalent moderation length λ [19]. The distributions of λ for three different E_n decades is illustrated in Figure 14. It is apparent that the distributions

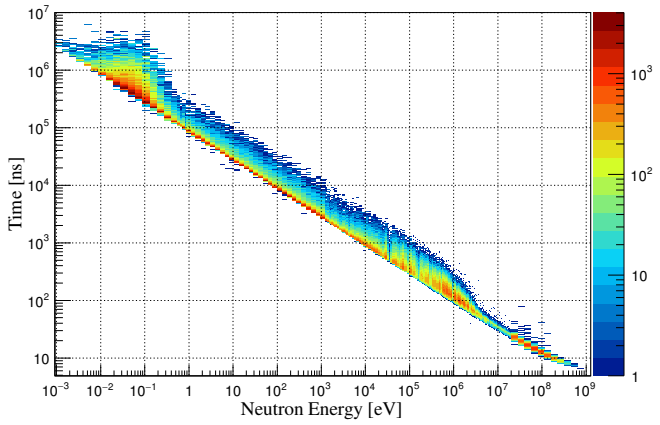

Figure 13: TOF to E_n relation at 1.5 m above the n_TOF spallation target, when the proton beam width is not considered. The number of simulated counts is encoded in color. Projections of the distributions at different E_n give the resolution functions of the vertical flight path.

widen with increasing E_n. For the distribution corresponding to $E_n = 1 - 10$ eV, a shoulder is appreciable on the distribution, which is still observable for the range $E_n = 0.1 - 1$ keV. This is caused by moderation processes in the different material layers at the target (Al, H_2O, Air).

Extensive simulations are yet to come for the final determi-

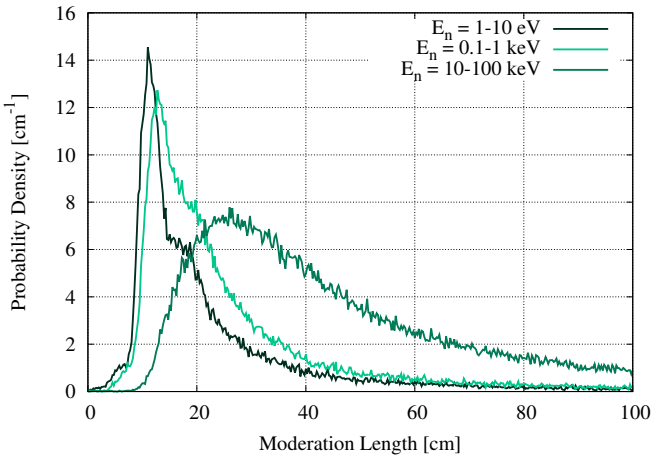

Figure 14: Moderation length distributions for three different E_n-decades at the vertical flight path. The shoulder on the distributions at lower E_n are due to moderation processes in the materials surrounding the spallation target.

nation of the resolution functions for the vertical flight path, where the shape of the tails will have to be studied in detail for small E_n-ranges. The neutron energy resolution can be defined via the relation

$$\left(\frac{\Delta E_n}{E_n}\right)^2 = \left(\frac{2\Delta\lambda}{\lambda + L}\right)^2 + \left(\frac{2\Delta T}{T}\right)^2, \quad (1)$$

where $\Delta\lambda$ is defined as the FWHM of the distributions in the different neutron energy ranges. ΔT represents the time spread of the impinging primary proton beam, which dominates the neutron energy resolution for $E_n > 10$ MeV. The currently available

simulation results are still too limited in statistics and hence only allow to give a first estimation of the neutron energy resolution at the experimental area of the vertical flight path. If the influence of the proton beam width is disregarded the neutron energy resolution is expected to be

- $\Delta E_n/E_n \approx 4\text{x}10^{-3}$ at $E_n = 1$ eV.
- $\Delta E_n/E_n \approx 4\text{x}10^{-2}$ at $E_n = 1$ MeV.

The corresponding values for the neutron energy resolution at the horizontal flight path are $3.2\text{x}10^{-4}$ and $5.3\text{x}10^{-3}$ for 1 eV and 1 MeV respectively [4]. The difference in neutron energy resolution of about one order of magnitude between the two flight paths is coherent with the difference in flight path length between the two areas, 20 m versus 200 m.

4. Summary and Conclusions

The new vertical flight path at the n_TOF facility at CERN was constructed in order to extend the experimental capabilities at this facility to very challenging cross-section measurements, i.e. for small mass or for high-activity radioactive samples. It is in operation and under commissioning since summer 2014. In this paper the technical design of the beam line and the expected performance in the new experimental station were presented.
The experimental area at this new vertical beam line is located 18 m above the Pb-spallation target. The neutron beam is shaped by two collimators in the beam line, where the exit diameter of the 2^{nd} collimator is 21.8 mm. Charged particles coming from spallation processes in the target, are deflected from the beam by a permanent dipole magnet with 0.287 Tm, located 10 m above the spallation target. A neutron filter station is as well available in this beam line to blank out certain neutron energies from the neutron spectrum. To achieve optimal background conditions, a sophisticated shielding system was implemented around the beam line and inside the experimental room.
The beam line design was based on extensive FLUKA Monte Carlo simulations. The new flight path offers a neutron spectrum from thermal neutron energies up to hundreds of MeV with a very high instantaneous flux. The integrated neutron flux is $1.1\text{x}10^7$ neutrons per $7\text{x}10^{12}$ protons impinging on target. The neutron flux at the vertical flight path is significantly higher than the available flux at the horizontal flight path at n_TOF for a comparable beam size, where the maximum neutron gain, with a factor 26, is available for $1 < E_n < 10$ keV. The neutron beam profile changes strongly as a function of distance from the floor of the experimental room. At the nominal sample position 1.6 m above the floor, the projected beam profile has FWHM = 21 mm for thermal neutron energies. With all shielding elements installed in the beam line, the neutron background outside the beam halo is 4 - 5 orders of magnitude smaller than the neutron flux at the peak of the beam profile. The expected background conditions for cross-section measurements from in-beam γ and the contributions of the different beam line elements have been estimated by means of FLUKA simulations. The in-beam photon energy spectra is dominated by the $E_\gamma = 2.2$ MeV energy in the delayed γ-spectrum. The expected neutron energy resolution is $\Delta E_n/E_n \approx 4\text{x}10^{-3}$ at $E_n = 1$ eV. Consistent with the difference in flight path length, the neutron energy resolution is approximately one order of magnitude better in the horizontal flight path of 200 m at n_TOF.

5. Acknowledgements

The authors greatly acknowledge the contribution of the following CERN groups: EN-STI, EN-MEF, EN-HE, EN-HDO, EN-CV, EN-EL, DGS-RP, DGS-SEE, GS-SE, GS-ASE, BE-ASR, TE-VSC, TE-MSC, PH-DI.

References

[1] C. Rubbia et al., *A high Resolution Spallation driven Facility at the CERN-PS to measure Neutron Cross Sections in the Interval from 1 eV to 250 MeV*, CERN/LHC/98-002-EET (1998)
[2] http://public.web.cern.ch/public/en/research/NTOF-en.html
[3] J.-P. Burnet et al., *Fifty years of the CERN Proton Synchrotron: Volume 1*, CERN-2011-04, (2011).
[4] C. Guerrero et al., *Performance of the neutron time-of-flight facility n_TOF at CERN*, Eur. Phys. J. A, 49:27, (2013).
[5] F. Gunsing et al., *Measurement of resolved resonances of ^{232}Th(n,γ) at the n_TOF facility at CERN*, Phys. Rev. C 85, 064601 (2012).
[6] C. Guerrero et al., *Investigation of Neutron-induced Reactions at n_TOF: an Overview of the 2009-2012 Experimental Program*, Nuclear Data Sheets 119, 5-9 (2014).
[7] M. Calviani et al., *Neutron-induced fission cross section of ^{245}Cm: New results from data taken at the time-of-flight facility n_TOF*, Phys. Rev. C 85, 034616 (2012).
[8] C. Paradela et al., *High-accuracy determination of the ^{238}U/^{235}U fission cross section ratio up to $\approx$ 1 GeV at n_TOF at CERN*, Phys. Rev. C 91, 024602 (2015).
[9] E. Chiaveri et al., *Proposal for n_TOF Experimental Area 2 (EAR-2)*, CERN-INTC-2012-029, INTC-O-015 (2012). D. Tarrio et al., *Measurement of the angular distribution of fission fragments using a PPAC assembly at CERN n_TOF*, NIMA 743, 79-85 (2014).
[10] P. Thonet, *CERN experience on PM based magnet design and procurement*, Workshop on Special Compact and Low Consumption Magnet Design, (2014).
[11] Le Conseil fdral suisse, *Ordonnance sur la radioprotection (ORaP)*, RS 814.501 (1994).
[12] I. Bergström, *Minimizing the background radiation in the new neutron time-of-flight facility at CERN: FLUKA Monte Carlo simulations for the optimization of the n_TOF second experimental line*, Master Thesis Luleå University of Technology, Sweden, CERN-THESIS-2013-203, LTU-EX-2013-43231076 (2013)
[13] S. Barros, *Neutron spectrometry and dosimetry for radiological protection using the n_TOF spectrometer at CERN*, PhD Thesis, Universidade Técnica de Lisboa, Portugal (2015).
[14] T.T. Bohlen et. al., *The FLUKA Code: Developments and Challenges for High Energy and Medical Applications*, Nuclear Data Sheets 120, 211-214 (2014).
[15] A. Ferrari et al., *FLUKA: a multi-particle transport code*, CERN-2005-10, INFN/TC_05/11, SLAC-R-773 (2005).
[16] V. Vlachoudis, *FLAIR: A Powerful But User Friendly Graphical Interface For FLUKA*, Proc. Int. Conf. on Mathematics, Computational Methods & Reactor Physics (M&C), New York (2009).
[17] *Règles Générales d'Exploitation*, CERN RGE section 9/S3-GSI1 (2006).
[18] S. Barros et al., *Optimization of n_TOF-EAR2 using FLUKA*, Journal of Instrumentation, accepted for publication (2015).
[19] G. Lorusso et al., *Time-energy relation of the n_TOF neutron beam: energy standards revisited*, Nucl. Instr. and Meth. in Phys. Res. A 532 (2004), p. 622.